

Article

Cu/Zn/Zr/Ga Catalyst for Utilisation of Carbon Dioxide to Methanol—Kinetic Equations

Łukasz Hamryszak ^{1,*}, Maria Madej-Lachowska ^{2,*} , Mirosław Grzesik ^{1,*} and Michał Śliwa ³ ¹ Institute of Chemical Engineering, Polish Academy of Sciences, 5 Bałtycka Street, 44-100 Gliwice, Poland² Department of Biosystem Engineering and Chemical Processes, Opole University of Technology, 31 Sosnkowskiego Street, 45-272 Opole, Poland³ Jerzy Haber Institute of Catalysis and Surface Chemistry, Polish Academy of Sciences, 8 Niezapominajek Street, 30-239 Krakow, Poland; ncsliva@cyf-kr.edu.pl

* Correspondence: lukasz.hamryszak@iich.gliwice.pl (Ł.H.); m.madej-lachowska@po.edu.pl (M.M.-L.); mgrzesik@gmail.com (M.G.)

Abstract: This paper presents the kinetics of methanol synthesis from carbon dioxide and hydrogen over a Cu/Zn/Zr/Ga catalyst. Kinetic studies were carried out in a continuous-flow fixed-bed reactor in a temperature range from 433 to 513 K, pressures from 3 to 8 MPa, and GHSV from 1660 to 10,000 1/h for initial molar fractions of hydrogen from about 0.48 to 0.70, carbon dioxide from 0.05 to about 0.22, and carbon monoxide from 0 to about 0.07. Significant effects of temperature and the composition of the reaction mixture on the conversion degrees α_1 and α_2 were found. The Cu/Zn/Zr/Ga catalyst showed good stability over 960 h. XRD and CO₂TPD characterisation were performed. The finally obtained results of kinetic tests were developed in the form of Langmuir–Hinshelwood kinetic equations. The numerical Levenberg–Marquardt method was used to estimate the kinetic equations. The average relative error of fitting the kinetic equations to the experimental data was 18%.



Citation: Hamryszak, Ł.; Madej-Lachowska, M.; Grzesik, M.; Śliwa, M. Cu/Zn/Zr/Ga Catalyst for Utilisation of Carbon Dioxide to Methanol—Kinetic Equations. *Catalysts* **2022**, *12*, 757. <https://doi.org/10.3390/catal12070757>

Academic Editor: Kuan Chang

Received: 30 May 2022

Accepted: 4 July 2022

Published: 9 July 2022

Publisher's Note: MDPI stays neutral with regard to jurisdictional claims in published maps and institutional affiliations.



Copyright: © 2022 by the authors. Licensee MDPI, Basel, Switzerland. This article is an open access article distributed under the terms and conditions of the Creative Commons Attribution (CC BY) license (<https://creativecommons.org/licenses/by/4.0/>).

Keywords: CO₂ hydrogenation; methanol synthesis; Cu/Zn/Zr-based catalyst; chemical kinetic; carbon dioxide utilisation

1. Introduction

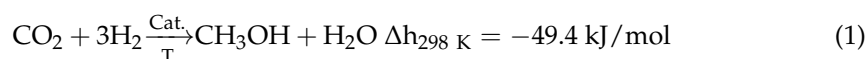
Global warming caused, among other things, by the increase in the carbon dioxide (CO₂) concentration in the atmosphere (from 381 ppm in 2006 to 427 ppm in 2021) and the depletion of fossil fuels, i.e., natural gas, oil, and coal, is becoming a huge challenge for modern society [1]. The continuous growth of CO₂ emissions (reaching 37 billion t in 2019) is caused by the rapid development of the global economy. There are numerous sources thereof, among which are the energy, heating, and chemical industries. In order to reduce the CO₂ content in the atmosphere, two methods [2] for its utilisation have been developed and implemented: carbon capture and storage (sequestration) (CCS) and carbon capture and utilisation (CCU), as well as CO₂ methanation [3–5]. The catalytic conversion of CO₂ to methanol is a promising and environmentally friendly route that can help solve the problem of managing and disposing of excess anthropogenic CO₂ and reducing the exploitation of fossil fuels [6].

Methanol is an important chemical compound with a wide range of applications in many industries including chemicals, plastics, fuel, and energy [7–9]. Between 2016 and 2021, its global consumption increased by 5%, reaching 110 million tonnes [10]. In the chemical industry, methanol is a resource for a wide range of chemicals, including formaldehyde, dimethyl ether, acetic acid, methanol-to-olefins (MTOs) and methanol-to-aromatics (MTAs) [11–14]. Furthermore, methanol is one of the liquid “green energy carriers”; it can be converted by decomposition or steam reforming into hydrogen, e.g., to power fuel cells [15]. On the industrial scale, methanol is mainly produced from synthesis gas

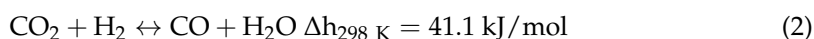
(CO/H₂) with a small addition of CO₂ (about 6 vol%) [16]; the process is carried out in the temperature range of 523–573 K and pressure range of 5–10 MPa in the presence of a Cu/ZnO/Al₂O₃ catalyst [11]. Since the late 1990s, attempts have been made to produce methanol straight from carbon dioxide and hydrogen on an industrial scale. The first pilot systems were established in Japan and Iceland [17–19]. The methanol production capacity of these installations is within the range of 0.05–400 t/year [18,19]. The methanol production from CO₂ and H₂ at the pilot plant in Japan is carried out on a modified Cu/Zn catalyst, at a pressure of 5 MPa and at a temperature of 523 K [18]. In 2012, Carbon Recycling International (CRI) in Reykanes, Iceland was the only company in the world to undertake larger-scale methanol production directly from CO₂ hydrogenation on a Cu/Zn/Al catalyst (KATALCO™) using geothermal sources to generate the electricity required for the process [19]. The methanol production of 400 t/year there is consuming 1.4 t CO₂/t_{MeOH}, and it consumes about 15,000 t less water than biomass methanol production [19,20]. It should be emphasised that the raw methanol obtained directly from CO₂ and H₂ shows much higher purity compared to the traditional method of its production from syngas [21].

The chemical reactions in the methanol synthesis process using CO₂ proceed according to the equations [17]:

direct methanol synthesis from carbon dioxide and hydrogen



reverse water–gas shift reaction (RWGS)



The reaction (1) is exothermic and (2) is endothermic.

The data in the literature suggest that the copper–zinc (Cu/Zn) (after prior reduction with hydrogen) is the system that plays a catalytic role in the methanol synthesis. According to existing hypotheses, zinc plays crucial role in improving the dispersion of copper atoms in the catalyst [22,23]. Improvement of activity and resistance to high content of carbon dioxide (much >6 vol.%) in Cu/Zn catalysts is achieved by its modification with oxides of various metals: aluminium [24,25], zirconium [26,27], chromium [28], gallium [29], and titanium [14]. Modification of Cu/Zn with zirconium oxide increases the tolerance of the catalyst to water, which is formed in reactions (1) and (2), and improves its stability and activity [26,27]. For a number of years, intensive attempts have been made to improve the Cu/Zn/Zr catalyst by introducing metal oxides: aluminium [30], boron [31], cerium [32–34], gallium [33–35], gadolinium [31], graphene (GO) [13], indium [31], lanthanum [32], magnesium [31], manganese [31], neodymium [32], palladium [34], praseodymium [32], silicon [32], tungsten [24], and yttrium [31]. These oxides cause, in most cases, a significant improvement in activity, lifetime, and resistance to increased CO₂ content, as well as a reduction in water adsorption on the catalyst surface that acts to inhibit the methanol formation. The activities of the catalysts were tested mostly in the temperature range 453–573 K and pressure range 2–8 MPa for gas hourly space velocity (GHSV) 3300–10,000 1/h, at a constant molar ratio of H₂ to CO₂ feed mixture of 3:1.

Available data in the literature concerning kinetic studies of methanol synthesis from carbon dioxide and hydrogen refer mainly to experiments carried out in the presence of a Cu/Zn/Al catalyst, under various conditions and for various compositions of the reaction mixture. Table 1 summarises selected kinetic equations and parameters of the methanol synthesis process described in the literature.

Table 1. Summary of selected kinetic equations proposed in the literature for methanol synthesis.

Ref.	Kinetic Equations	Operating Conditions		Feed Composition and Catalyst	Estimated Activation Energies (kJ/mol)
		T (K)	P _c (MPa)		
Graaf et al. [36]	$r_1 = k_1 K_{CO_2} \left[\frac{P_{H_2}^{1.5} P_{CO_2} - \frac{P_{MeOH} P_{H_2} O}{K_{eq1} P_{H_2}^{1.5}}}{\left(1 + K_{CO} P_{CO} + K_{CO_2} P_{CO_2}\right) \left(P_{H_2}^{0.5} + \frac{K_{H_2} O}{K_{H_2}^{0.5}} P_{H_2} O\right)} \right]$	483–516	1.5–5	H ₂ : 0.67–0.90 CO ₂ : 0.02–0.26 CO: 0.00–0.22 Cu/Zn/Al	E1 = 65 E2 = 123 E3 = 109
	$r_2 = k_2 K_{CO_2} \left[\frac{P_{H_2} P_{CO_2} - \frac{P_{CO} P_{H_2} O}{K_{eq2}}}{\left(1 + K_{CO} P_{CO} + K_{CO_2} P_{CO_2}\right) \left(P_{H_2}^{0.5} + \frac{K_{H_2} O}{K_{H_2}^{0.5}} P_{H_2} O\right)} \right]$				
	$r_3 = k_3 K_{CO} \left[\frac{P_{H_2}^{1.5} P_{CO} - \frac{P_{MeOH}}{K_{eq3} P_{H_2}^{1.5}}}{\left(1 + K_{CO} P_{CO} + K_{CO_2} P_{CO_2}\right) \left(P_{H_2}^{0.5} + \frac{K_{H_2} O}{K_{H_2}^{0.5}} P_{H_2} O\right)} \right] \quad a$				
Malinovskaya et al. [37]	$r_1 = \frac{k_1 P_{H_2} P_{CO_2} \left(1 - \frac{P_{MeOH} P_{H_2} O}{P_{H_2}^3 P_{CO_2} K_{eq1}}\right)}{P_{CO_2} + b_{H_2} O P_{H_2} O P_{CO_2} + b' P_{H_2} O}$	473–553	5–10	H ₂ : 0.60–0.90 CO ₂ : 0.01–0.26 CO: 0.01–0.1 Cu/Zn/Al (SNM-3)	E1 = 69 E2 = 66
	$r_2 = \frac{k_2 P_{H_2} P_{CO_2} \left(1 - \frac{P_{CO} P_{H_2} O}{P_{H_2} P_{CO_2} K_{eq2}}\right)}{P_{CO_2} + b_{H_2} O P_{H_2} O P_{CO_2} + b' P_{H_2} O}$				
Skrzypek et al. [38]	$r_1 = k_1 K_{H_2}^2 K_{CO_2} \left[\frac{P_{H_2}^2 P_{CO_2} - \frac{P_{CH_3} OH P_{H_2} O}{K_{eq1} P_{H_2}}}{\left(1 + K_{H_2} P_{H_2} + K_{CO_2} P_{CO_2} + K_{CH_3} OH P_{CH_3} OH + K_{CO} P_{CO} + K_{H_2} O P_{H_2} O\right)^3} \right]$	460–550	3–9	H ₂ : 0.10–0.80 CO ₂ : 0.05–0.35 CO: 0.00–0.20 Cu/Zn/Al (Błasiaka)	E1 = 105 E2 = 105
	$r_2 = k_2 K_{H_2} K_{CO_2} \left[\frac{P_{H_2} P_{CO_2} - \frac{P_{CO} P_{H_2} O}{K_{eq2}}}{\left(1 + K_{H_2} P_{H_2} + K_{CO_2} P_{CO_2} + K_{CH_3} OH P_{CH_3} OH + K_{CO} P_{CO} + K_{H_2} O P_{H_2} O\right)^2} \right]$				

Table 1. Cont.

Ref.	Kinetic Equations	Operating Conditions		Feed Composition and Catalyst	Estimated Activation Energies (kJ/mol)
		T (K)	Pc (MPa)		
VandenBussch and Froment [39]	$r_1 = \frac{k'_{\text{MeOH}} P_{\text{H}_2} P_{\text{CO}_2} \left(1 - \frac{1}{K_{\text{eq1}}} \frac{P_{\text{MeOH}} P_{\text{H}_2} \text{O}}{P_{\text{H}_2}^3 P_{\text{CO}_2}}\right)}{\left(1 + K_{\text{redox}} \frac{P_{\text{H}_2} \text{O}}{P_{\text{H}_2}} + \sqrt{K_{\text{H}_2} P_{\text{H}_2} + K_{\text{H}_2} \text{O} P_{\text{H}_2} \text{O}}\right)^3}$ $r_2 = \frac{k_2 P_{\text{CO}_2} \left(1 - K_{\text{eq2}} \frac{P_{\text{CO}} P_{\text{H}_2} \text{O}}{P_{\text{H}_2} P_{\text{CO}_2}}\right)}{\left(1 + K_{\text{redox}} \frac{P_{\text{H}_2} \text{O}}{P_{\text{H}_2}} + \sqrt{K_{\text{H}_2} P_{\text{H}_2} + K_{\text{H}_2} \text{O} P_{\text{H}_2} \text{O}}\right)}$	453–533	1.5–5.1	H ₂ : 0.7 CO ₂ : 0.00–0.30 CO: 0.00–0.30 Cu/Zn/Al (ICI 51-2)	E1 = −37 E2 = 95
Kubota et al. [40]	$r_1 = \frac{k_1 P_{\text{H}_2} P_{\text{CO}_2} \left(1 - \frac{1}{K_{\text{eq1}}} \frac{P_{\text{MeOH}} P_{\text{H}_2} \text{O}}{P_{\text{H}_2}^3 P_{\text{CO}_2}}\right)}{\left(1 + K_{\text{CO}_2} P_{\text{CO}_2} + K_{\text{H}_2} \text{O} P_{\text{H}_2} \text{O}\right)^2}$ $r_2 = \frac{k_2 P_{\text{CO}_2} \left(1 - \frac{1}{K_{\text{eq2}}} \frac{P_{\text{CO}} P_{\text{H}_2} \text{O}}{P_{\text{H}_2} P_{\text{CO}_2}}\right)}{\left(1 + K_{\text{CO}_2} P_{\text{CO}_2} + K_{\text{H}_2} \text{O} P_{\text{H}_2} \text{O}\right)}$	473–548	4.9	H ₂ : 0.75 CO ₂ : 0.22 CO: 0.03 Cu/Zn/Zr/Al/Si	E1 = 32 E2 = 113
Ladera et al. [35]	$r_1 = k_1 P_{\text{H}_2}^{1.18} P_{\text{CO}_2}^{0.53}$ $r_2 = k_2 P_{\text{H}_2}^{0.15} P_{\text{CO}_2}^{0.67}$	463–523	0.3–4.2	– Cu/Zn/Zr/Ga	E1 = 31 E2 = 111

^a CO + 2H₂ ↔ CH₃OH.

Graaf et al. [36] presented kinetic equations for methanol synthesis based on the Langmuir–Hinshelwood mechanism, considering the reactions of hydrogenation of carbon dioxide (1) and carbon monoxide ($\text{CO} + 2\text{H}_2 \leftrightarrow \text{CH}_3\text{OH}$) to methanol as well as the accompanying RWGS reaction (2). The experiments were carried out in a spinning basket reactor. Graaf's equations are the most commonly used kinetic models in industrial practice [41,42].

Malinovskaya et al. [37] conducted kinetic studies of methanol synthesis considering only reactions (1) and (2). These experiments were conducted in the flow reactor, using a Cu/Zn/Al industrial catalyst (SNM-3) at $T = 473\text{--}553\text{ K}$ and $p = 5\text{--}10\text{ MPa}$ including the effect of CO_2 and CO concentrations (Table 1). The fit of the kinetic equations to the experimental data was about 10%.

Skrzypek et al. [38] carried out a full kinetic study of methanol synthesis in a continuous-flow fixed-bed reactor with an industrial Cu/Zn/Al catalyst (Błasiak catalyst). This study extensively considered the effects of temperature and pressure and the different initial composition of the reaction mixture on the reaction rates (1) and (2) (Table 1). The kinetic equations developed were based on 70 measurement points and took into account the possibility of the occurrence of maxima in the relationship between the reaction rates (1) and (2) and the inlet concentrations of CO_2 and H_2 (in the absence of CO at the reactor inlet). The proposed kinetic equations correspond to Langmuir–Hinshelwood sequences with the surface reaction between hydrogen and carbon dioxide as the rate-limiting step. In preliminary studies that preceded the kinetic studies, it was found that methanol in the presence of the copper catalyst used was formed from CO_2 and not from CO.

Vanden Bussche and Froment [39] carried out a full kinetic investigation of methanol synthesis in a continuous-flow fixed-bed reactor with the Cu/Zn/Al industrial ICI catalyst. These studies included determining the effects of temperature, pressure, and composition of the initial reaction mixture on the reaction rate (Table 1). The mass balance equations with the proposed kinetic equations based on reactions (1) and (2) were integrated using the numerical method of Runge and Kutta IV and V, and the calculated values of the transformation rates were compared with the experimental values. Nine parameters were estimated simultaneously using the Levenberg and Marquard nonlinear regression method. A good agreement of the model fit to the experimental data was obtained over the range of parameters studied.

A very good model fit to their experimental data (30 points), which did not exceed 10%, was obtained by Kubota et al. [40]. This team developed kinetic equations for methanol synthesis based on data obtained from a continuous-flow fixed-bed reactor with a Cu/Zn/Zr/Al/Si catalyst. These equations were developed under the assumptions that methanol is formed from the transformation of intermediates (including HCOO^*), the rate-limiting step in the overall process being the surface reaction between intermediates adsorbed on the catalyst surface and hydrogen atoms. Furthermore, it was assumed that the RWGS reaction (2) occurs by direct decomposition of CO_2 to CO on the Cu surface. In the denominator of both equations, the partial pressure of hydrogen was omitted because of the small change, and the quotient of the partial pressure of water to hydrogen was omitted because it is less than zero.

Ladera et al. [35] carried out an activity investigation of the Cu/Zn/Zr/Ga catalyst and an incomplete kinetic study of methanol synthesis in a continuous-flow fixed-bed reactor, determining the effects of temperature and pressure on the reaction rate. It was found that above about 520 K the rate of the RWGS reaction increases, while high CO_2 partial pressures ($>1.25\text{ MPa}$) favour the reaction (1). Ladera et al. [35] suggest that the hydrogenation of CO_2 to methanol can occur according to the Eley–Rideal mechanism. Furthermore, based on the obtained kinetic results for reactions (1) and (2), this group determined the kinetic equations in power monomial form, and estimated its parameters without considering the sorption terms (Table 1).

Kinetic investigations presented in the literature mainly concern methanol synthesis on a Cu/Zn/Al catalyst. This catalyst, as mentioned previously, is not resistant to high CO_2 content and the presence of water in the reaction mixture. The aim of this work is

to estimate the kinetics of methanol synthesis from carbon dioxide and hydrogen on a copper-zinc-zirconium catalyst modified with gallium oxide. The scope of the research includes the investigation of the influence of temperature, pressure, reactant flow rate, and initial composition of substrates on the course of methanol synthesis on a Cu/Zn/Zr/Ga catalyst. The final activity of the kinetic investigations of methanol synthesis was to estimate the kinetic equations and its parameters (pre-exponential constants, activation energies, sorption constants).

2. Results and Discussion

2.1. Characteristics of the Catalyst

The structures of the fresh and spent Cu/Zn/Zr/Ga catalyst were compared using XRD (Figure 1).

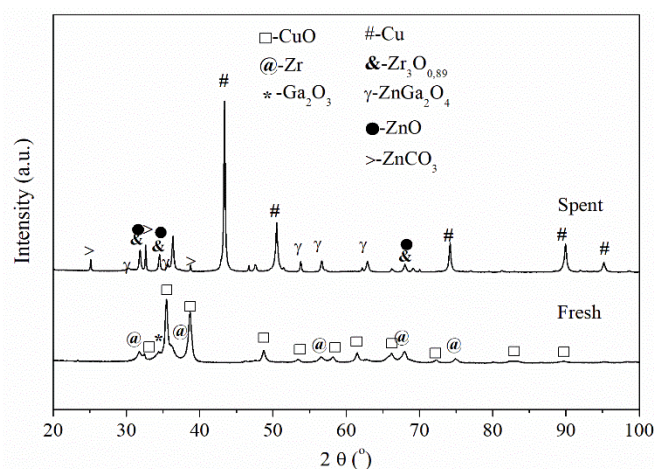


Figure 1. XRD patterns of the fresh and spent Cu/Zn/Zr/Ga catalyst.

Analysis of the XRD diffractograms (Figure 1) of the fresh Cu/Zn/Zr/Ga catalyst indicates the presence of CuO, which corresponds to an intense peak (at $2\theta = 35$ and 38°) and weakly intense peaks of zirconium (at $2\theta = 31$, 55 and 67°) and Ga_2O_3 ($2\theta = 34^\circ$), among others. It is worth mentioning that the spectrum of the fresh Cu/Zn/Zr/Ga catalyst shows the presence of an amorphous phase and a weakly developed crystalline phase [32]. The spectrum of the spent Cu/Zn/Zr/Ga catalyst shows an intense band characteristic of metallic Cu (i.e., around $2\theta = 43$ and 50°) and a weak intensity of spinel ZnGa_2O_4 ($2\theta = 54$, 56 and 62°) and ZnCO_3 ($2\theta = 25$, 33 and 39°). The spent catalyst shows increased phase crystallinity.

Crystallite sizes calculated using the Scherrer method and basic parameters of the porous structure of the Cu/Zn/Zr/Ga catalyst are presented in Table 2.

Table 2. Cu/Zn/Zr/Ga composition, textural properties, and crystallite size.

CuO (Mass%)	ZnO (Mass%)	Other Metal Oxides ^a (Mass%)	Size of Crystallites (nm)		S_{Cu}^c ($\text{m}^2/\text{g}_{\text{Cu}}$)	S_{BET}^d (m^2/g)	V_p (cm^3/g)	D_p (nm)	Ref.
			Fresh CuO (111)	Spent ^b Cu ⁰ (111)					
65.3	26.3	8.4	9.7	29.6	8.7	29	0.09	12	Present work
61.0	31.0	8.0	14.5	16.1	–	21	–	–	[31]
50.0	15.0	35.0	–	7.0	13.5	102	–	–	[35]
39.0	29.0	32.0	–	12.7	57.1	143	–	–	[43]

^a ZrO_2 , Ga_2O_3 ; ^b after kinetic studies; ^c measured by dissociative N_2O adsorption; ^d measured by N_2 adsorption at 77 K.

The BET and S_{Cu} surface area for the investigated catalyst are markedly lower than those presented by the Ladera [35] and Natesakhawat [43] groups, which may be due to the different method of catalyst preparation.

The CO₂TPD experiment was performed in order to evaluate the surface basicity of the synthesized catalyst. The recorded TPD profile (Figure 2) was analysed in the temperature range corresponding with the temperature at which the methanol synthesis had been carried out.

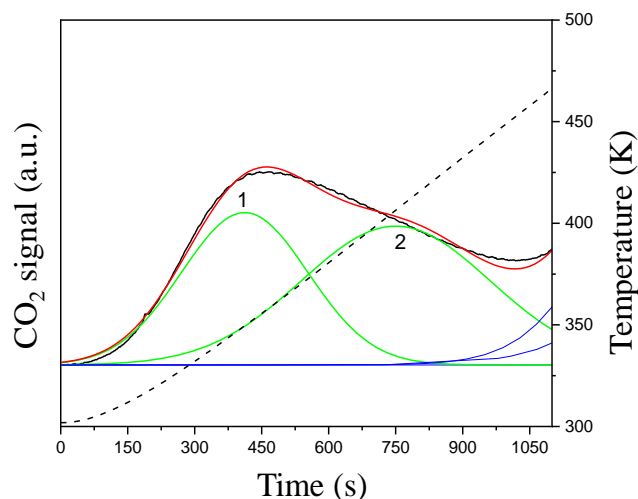


Figure 2. CO₂TPD profile for Cu/Zr/Zn/Ga catalyst: signal—black line, cumulative curve—red line, deconvoluted peaks used for quantification—green line, temperature—dashed line (For interpretation of the references to colour in this figure legend, the reader is referred to the Web version of this article).

In the recorded CO₂TPD profile (Figure 2) for the Cu/Zr/Zn/Ga catalyst, the desorption signal in the low temperature range is visible. The position of deconvoluted peaks 1 and 2, which is between 323 K and 423 K, shows that solely weak basic sites are present on the surface of the Cu/Zr/Zn/Ga [44]. The total basicity is low and equal to 15.5 $\mu\text{mol/g}_{\text{cat}}$. (Table 3).

Table 3. Quantitative analysis of basic sites for Cu/Zn/Zr/Ga.

Catalyst	Peak	T_{max} (K)	Weak Basic Sites ($\mu\text{mol/g}_{\text{cat}}$)	$\text{Tot}_{\text{des}}/\text{Tot}_{\text{ads}}$	Total Basicity ($\mu\text{mol/g}_{\text{cat}}$)
Cu/Zn/Zr/Ga	1	348	6.6	0.97	15.5
	2	405	8.9		

The observed increase in the CO₂ line above ca. 470 K is related to the desorption of CO₂ that originates from the atmosphere [45,46]. This CO₂ was not removed upon sample activation prior to TPD because the temperature was not high enough. The contribution of atmospheric CO₂ in the TPD profile was marked with a blue line (Figure 2) and was not taken into consideration for the total basicity calculation. Additionally, the ratio of CO₂ desorbing in the temperature range 323–343 K (Tot_{des}) to adsorbed CO₂ via pulses (Tot_{ads}) is close to one (Table 3). This also shows that CO₂ desorbing at higher temperatures is atmospheric.

Thermogravimetric analysis of the spent Cu/Zn/Zr/Ga catalyst performed using a nitrogen and air atmosphere is presented in Figure 3a,b.

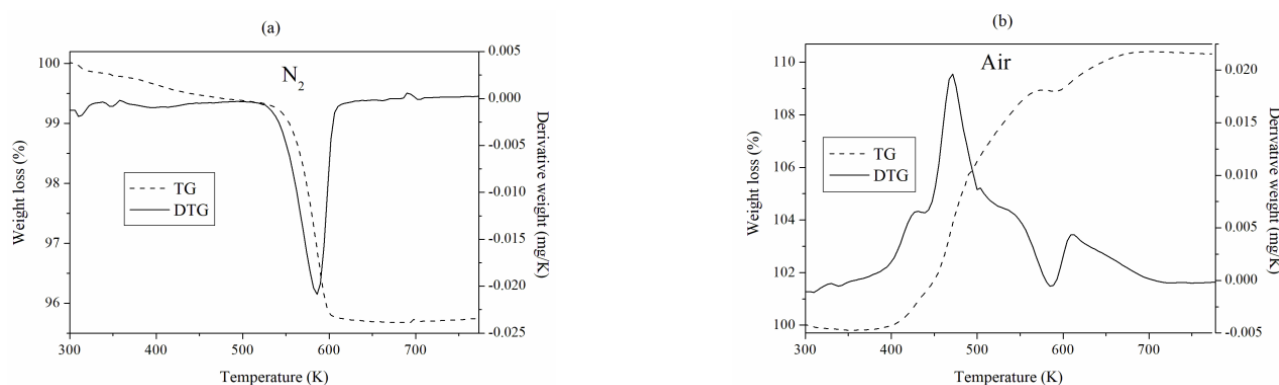


Figure 3. TG and DTG curves of Cu/Zn/Zr/Ga reduced, performed in the (a) N₂ and (b) air atmosphere.

Heating the Cu/Zn/Zr/Ga catalyst after kinetic studies to 773 K in an N₂ atmosphere resulted in a mass loss of about 5% in the 520–615 K range, associated with the decomposition of ZnCO₃ to ZnO and CO₂ at 573 K [47] (Figure 3a).

The DTG curve of the catalyst heated in the atmosphere of air (Figure 3b) shows a mass increase of about 8% in the range of 400–728 K. This growth is presumably related to the oxidation of the reduced active form of the catalyst, i.e., Cu⁰ + 0.5O₂ → CuO. The overlapping small mass loss at 586 K is associated with the decomposition of ZnCO₃ to ZnO and CO₂ [47,48]. The amount of O₂ calculated from DTG, assuming that there are no carbon deposits in the spent catalyst, indicates that 85 wt.% of copper was in the reduced form Cu⁰. Since the presence of a carbon deposit in the spent catalyst cannot be excluded, part of the oxygen was certainly used for its oxidation. Therefore, the amount of the reduced form Cu⁰ was smaller than 85 wt.%, but it cannot be precisely determined.

2.2. Kinetics Tests

The carried out kinetic tests yielded dozens of measurement points, which were used to plot kinetic curves, on the basis of which a preliminary analysis of the data was carried out in terms of the influence of process parameters on the reaction rate. The results of kinetic tests are presented in Figures 4–9 as curves of the dependence of the conversion degrees α_1^{exp} and α_2^{exp} on temperature, pressure, GHSV, and initial composition of the reaction mixture for reactions (1) and (2).

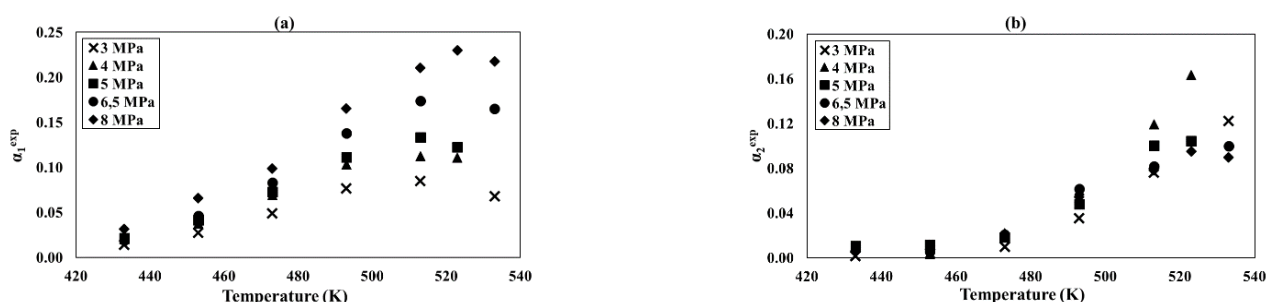


Figure 4. Relationship of the α_1^{exp} and α_2^{exp} conversion as a function of temperatures at the different total pressure: (a) reaction (1), (b) reaction (2), and process conditions: GHSV = 3300 1/h, $X_{\text{H}_2}^0 = 0.69$, and $X_{\text{CO}_2}^0 = 0.21$.

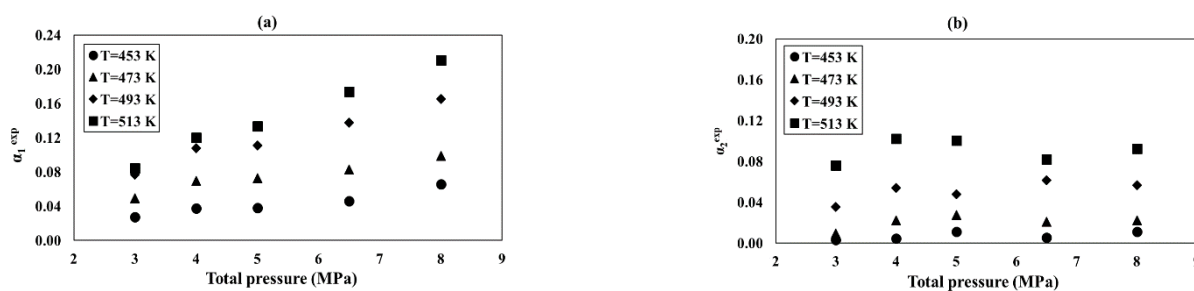


Figure 5. Relationship of the α_1^{exp} and α_2^{exp} conversion as a function of total pressure at the different temperatures: (a) reaction (1), (b) reaction (2), and process conditions: GHSV = 3300 1/h, $X_{H_2}^0 = 0.69$, and $X_{CO_2}^0 = 0.21$.

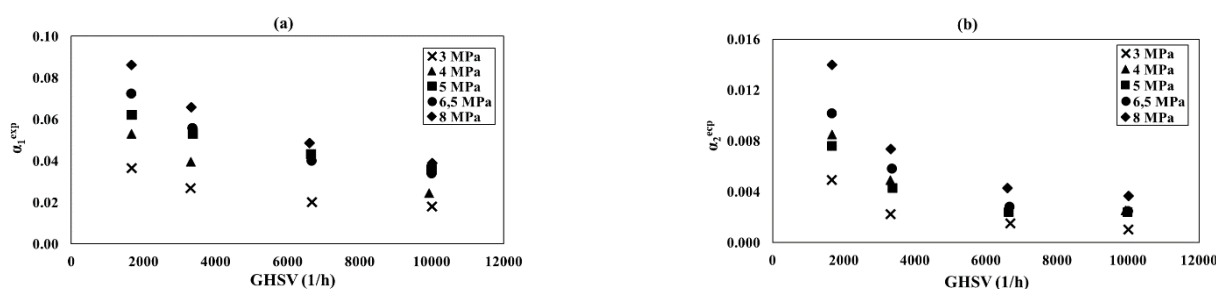


Figure 6. Relationship of the α_1^{exp} and α_2^{exp} conversion as a function of GHSV at the different total pressure amounts: (a) reaction (1), (b) reaction (2), and process conditions: $X_{H_2}^0 = 0.69$ and $X_{CO_2}^0 = 0.21$.

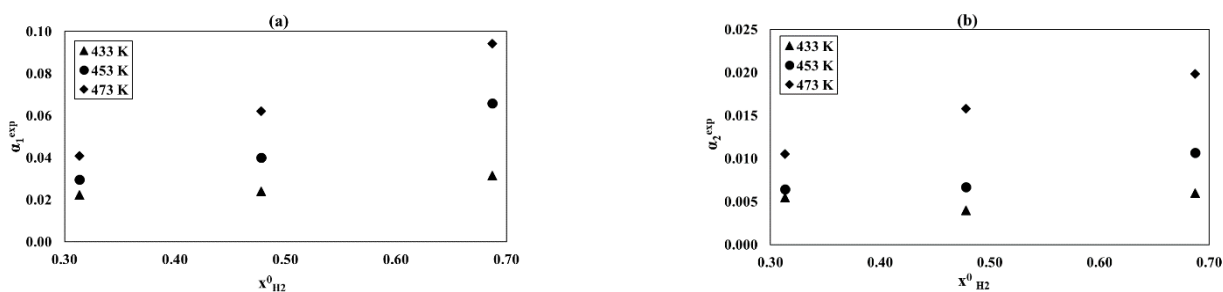


Figure 7. Relationship of the α_1^{exp} and α_2^{exp} conversion as a function of initial hydrogen concentrations at the different temperatures: (a) reaction (1), (b) reaction (2), and process conditions: $p = 8$ MPa, GHSV = 3300 1/h, and $X_{CO_2}^0 = 0.20$.

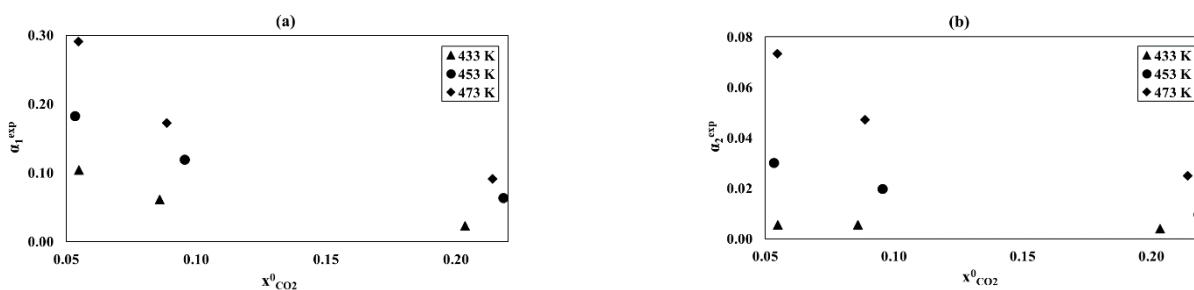


Figure 8. Relationship of the α_1^{exp} and α_2^{exp} conversion as a function of initial carbon dioxide concentrations at the different temperatures: (a) reaction (1), (b) reaction (2), and process conditions: $p = 8$ MPa, GHSV = 3300 1/h, and $X_{H_2}^0 = 0.69$.

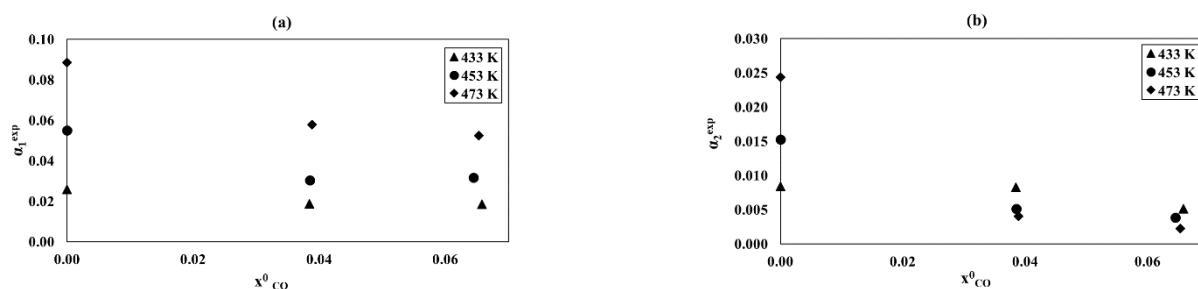


Figure 9. Relationship of the α_1^{exp} and α_2^{exp} conversion as a function of initial carbon oxide concentrations at the different temperature: (a) reaction (1), (b) reaction (2), and process conditions: $p = 8$ MPa, GHSV = 3300 1/h, $X_{\text{H}_2}^0 = 0.68$, and $X_{\text{CO}_2}^0 = 0.22$.

Figure 4a,b shows the temperature relationships of the conversion degrees α_1^{exp} and α_2^{exp} for different pressures. For both reactions, an about 90% increase in the conversion degrees α_1^{exp} and α_2^{exp} is observed in comparison to the initial values. For reaction (1), this influence declines with alower pressure of more than 50%. For reaction (2), this effect can be observed above a temperature of about 490 K (more than 30% change). It is important to mention that the methanol synthesis is an exothermic process, so further increase in temperature over 513 K is unfavourable, as reaction (2) is endothermic and becomes dominant, causing a decrease in the conversion degree of α_1^{exp} from 2 to 25% (Figure 3a).

Figure 5a,b shows the pressure relationships of the conversion degrees α_1^{exp} and α_2^{exp} for different temperatures. The pressure dependences of α_1^{exp} and α_2^{exp} are smaller than the effect of temperature (Figure 4a,b and Figure 5a,b). The conversion degree α_1^{exp} increases with the pressure by more than 50%, while α_2^{exp} is almost constant for all tested temperatures. The differences occur only within temperatures of 453–513 K and reach up to 50% (Figure 5b).

Figure 6a,b shows the GHSV relationships of the conversion degrees α_1^{exp} and α_2^{exp} for different pressures. For both, reactions α_1^{exp} and α_2^{exp} decrease with rising GHSV. This relationship appears to be stronger with higher pressure. Especially for the GHSV range 1660–3310 1/h, a decrease from about 5% to about 30% (α_2^{exp} for 8 MPa) occurs.

Figure 7a,b shows the dependence of the conversion degrees α_1^{exp} and α_2^{exp} on the initial hydrogen concentration for temperatures of 433, 453, and 473 K. The influence of the initial hydrogen concentration was studied at the constant of $X_{\text{CO}_2}^0$ equal to 0.20. An increase in α_1^{exp} and α_2^{exp} is observed for both reactions with increasing concentrations. This effect is more evident for higher temperatures.

Figure 8a,b shows the dependence of the conversion degrees α_1^{exp} and α_2^{exp} on the initial carbon dioxide concentration for temperatures of 433, 453, and 473 K. The effect of initial carbon dioxide concentration was determined at a constant initial hydrogen concentration equal to 0.69.

For both reactions, increasing CO_2 content caused a decrease even more than four-fold of α_1^{exp} and α_2^{exp} , as shown in Figure 8a,b. This effect is reversed and slightly weaker than for the hydrogen content (compare Figure 7a,b and Figure 8a,b). The largest reduction in α_1^{exp} , 70%, occurred for a temperature of 473 K (Figure 7a). Analysis of the effect of molar fractions of hydrogen and carbon dioxide on α_1^{exp} and α_2^{exp} indicated that the size of the S_{Cu} of the studied catalyst favours hydrogen adsorption, but negatively affects CO_2 adsorption, which in excess reduces its activity [49]. The excess of spherically large CO_2 molecules adsorbed on the catalyst surface, specifically on Zn and/or Zr oxides, blocks the access of much smaller H_2 molecules onto the Cu surface; thus, α_1^{exp} and α_2^{exp} can be reduced.

Figure 9a,b shows the dependence of the conversion degrees α_1^{exp} and α_2^{exp} on the initial carbon monoxide concentration for temperatures of 433, 453, and 473 K. The effect of the initial molar fraction of carbon monoxide was studied at constant initial concentrations of $\text{H}_2\text{X}_{\text{H}_2}^0 = 0.68$ and $\text{X}_{\text{CO}_2}^0 = 0.22$.

The presence of CO shifts the equilibrium state of the RWGS reaction towards the formation of CO_2 and the removal of the water, which is formed in reaction (1). This is beneficial for the process to be conducted because water can cause partial deactivation of the copper catalyst. The effect of the initial molar fraction of CO on reaction (1) is similar in nature to that of CO_2 . For reaction (2), the decrease in α_2^{exp} is more evident than for reaction (1), in particular at 473 K.

2.3. Stability

The catalyst should exhibit stable behaviour during operation. Its activity should not change; thus, it should be resistant to various factors (coking, sintering). In order to examine the stability, the dependence of α_1^{exp} and α_2^{exp} and the productivity as a function of time on stream were determined. The stability was checked for 1056 h by carrying out weekly measurements for identical process parameters: at a temperature of 453 K and pressure of 8 MPa, at a constant flow rate of 100 mL/min (GHSV = 3300 1/h) for a reaction mixture of 0.69 H_2 and 0.21 CO_2 (Figure 10). Up to 700 h of the measurements, small (within the measurement error) deviations of α_1^{exp} and α_2^{exp} values (marked as points in Figure 10) from their average values (lines in Figure 10) were observed for both reactions. After about 700 h of stable work, the beginning of a downward trend in productivity appears so that, for 1000 h, the decrease in productivity reaches about 20%. The part of CO_2 can be bonded to ZnO, leading to the formation of ZnCO_3 (Figures 1 and 3a,b). The CO_2 adsorption active centres were blocked, resulting in a decrease in productivity. The formation of ZnCO_3 is attributed to the prolonged residence of the catalyst at elevated pressure (8 MPa) [50]. In a study by Asha-Kurlander et al. [51] on methanol synthesis from H_2 and CO_2 , ZnCO_3 was found to be formed in an acidic environment, which is responsible for the partial dissolution of ZnO in a mixture of H_2O and CO_2 .

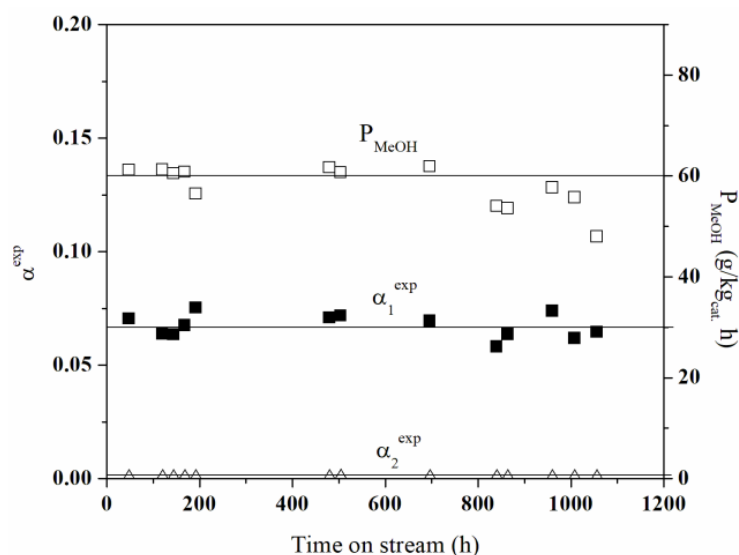


Figure 10. Relationship of the α_1^{exp} and α_2^{exp} conversion and productivity on the operating time for reactions (1) and (2), and process conditions: $T = 453$ K, $p = 8$ MPa, GHSV = 3300 1/h, $\text{X}_{\text{H}_2}^0 = 0.69$, and $\text{X}_{\text{CO}_2}^0 = 0.21$.

2.4. Kinetic Equations

The next step of our work was to determine the kinetic equations for methanol synthesis from CO₂ and H₂. The obtained results were developed in the form of kinetic equations of the Langmuir–Hinshelwood type with the surface reaction between CO₂ and H₂ as the limiting step:

$$r_1 = k_1 \cdot \left[\frac{P_{H_2}^2 \cdot P_{CO_2} - \frac{P_{CH_3OH} \cdot P_{H_2O}}{K_{eq1} \cdot P_{H_2}}}{\left(1 + K_{H_2} \cdot P_{H_2} + K_{CO_2} \cdot P_{CO_2} + K_{CH_3OH} \cdot P_{CH_3OH} + K_{CO} \cdot P_{CO} + K_{H_2O} \cdot P_{H_2O}\right)^3} \right] \quad (3)$$

$$r_2 = k_2 \cdot \left[\frac{P_{H_2} \cdot P_{CO_2} - \frac{P_{CO} \cdot P_{H_2O}}{K_{eq2}}}{\left(1 + K_{H_2} \cdot P_{H_2} + K_{CO_2} \cdot P_{CO_2} + K_{CH_3OH} \cdot P_{CH_3OH} + K_{CO} \cdot P_{CO} + K_{H_2O} \cdot P_{H_2O}\right)^2} \right] \quad (4)$$

where r_1 and r_2 (mol/(kg_{cat.}·h)) are, respectively, the rate of reactions (1) and (2) and k_n (mol/(kg_{cat.}·h)) is the rate constant of the n -th reaction expressed by the Arrhenius equation:

$$k_n = k_{on} \exp\left(-\frac{E_n}{RT}\right). \quad (5)$$

The partial pressures, p_i (MPa), of the i -th reactant ($i = H_2, CO_2, CH_3OH, CO, H_2O$) are defined as:

$$P_i = x_i P_c. \quad (6)$$

The sorption equilibrium constant, K_i (MPa), of the i -th reactant changes with temperature according to the equation:

$$K_i = K_{0i} \exp\left(\frac{\Delta H_i}{RT}\right). \quad (7)$$

The thermodynamic equilibrium constants of the n -th reaction ($K_{eq,n}$) were calculated from the formulas in the publication [52] and have the following form:

$$\log_{10}(K_{eq1}) = \frac{3217}{T} - 10.889, \quad (8)$$

$$\log_{10}(K_{eq2}) = \frac{1922}{T} - 1.732. \quad (9)$$

In the foregoing equations, a standard form of kinetic equations of the Langmuir–Hinshelwood type was assumed, including a kinetic group, a driving module of the process, and a sorption group. The kinetic group of these equations contains only the reaction rate constants k_1 and k_2 , while the sorption constants present in the equation of Skrzypek et al. [38] are not included. The sorption component takes into account all reagents involved in the present process. The values of exponents in Equations (3) and (4) were checked for the values proposed by Skrzypek et al. [38] ($a = 3$; $b = 2$), considering that these values were determined for slightly different systems of kinetic equations.

Figure 11a,b shows α^{cal} as a function of α^{exp} for 59 experimental data.

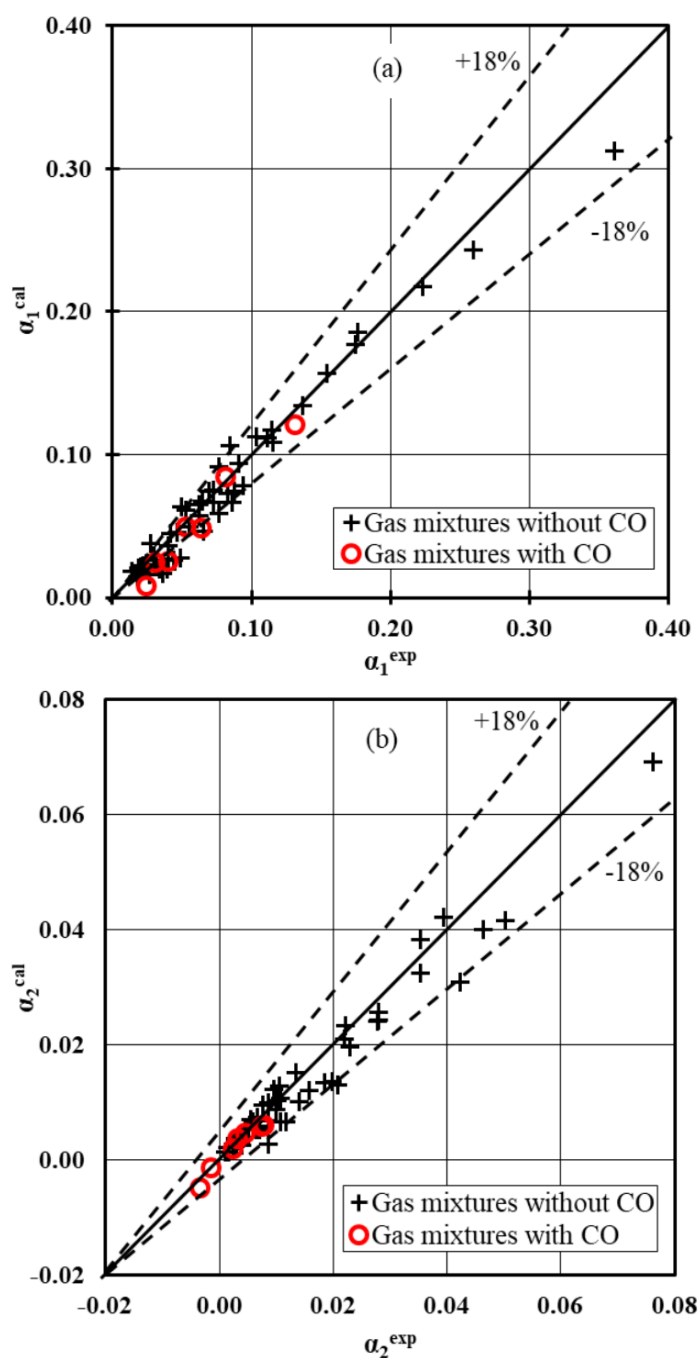


Figure 11. Parity plot for integral conversion: (a) α_1 and (b) α_2 .

The considered kinetic equations give the smallest difference between the experimental and calculated conversion degrees under the investigated process conditions on the Cu/Zn/Zr/Ga catalyst. For both high conversion degrees α_1^{exp} and α_2^{exp} a slight deviation of the points from the diagonal reaching only 10% is observed. It should be noted that the kinetic equations approximate the conversion degrees α_1^{exp} and α_2^{exp} with satisfactory accuracy for reaction mixtures containing small amounts of CO.

The fits of the experimental data and those calculated using the estimated kinetic equations, Equations (3) and (4), are shown in Figures 12a— α_1 and 12b— α_2 .

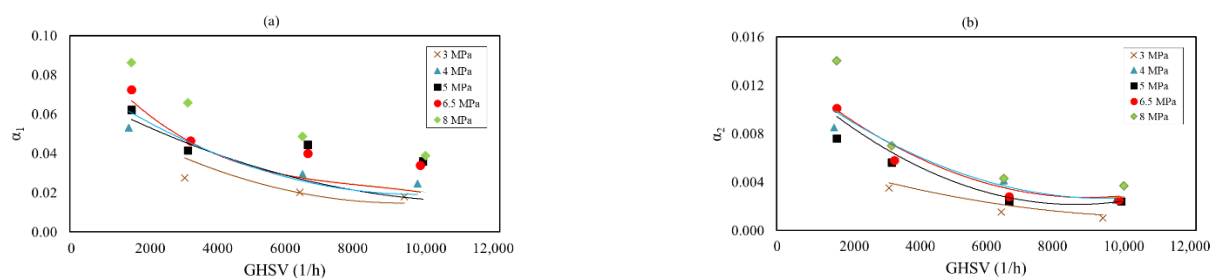


Figure 12. Relationships of the α_1 and α_2 conversions as a function of GHSV at the different total pressure values: (a) reaction (1), (b) reaction (2), and process conditions: $X_{H_2}^0 = 0.69$ and $X_{CO_2}^0 = 0.21$. The experimental data are the points, and the calculated data compose the line. (For interpretation of the references to colour in this figure legend, the reader is referred to the Web version of this article).

The proposed kinetic equations, Equations (3) and (4), fit the experimental data well, reflecting the decrease in conversion degrees α_1 and α_2 with increases in GHSV.

The values of the determined kinetic parameters are summarised in Table 4.

Table 4. The values of estimated kinetic parameters.

Reaction 1					Reaction 2				
k_{01} (mol/kg _{cat.} ·h)		E_1 (J/mol)			k_{02} (mol/kg _{cat.} ·h)		E_2 (J/mol)		
4.1×10^7		66,280			5.2×10^8		81,060		
Other parameters									
K_{0H_2} (1/MPa)	ΔH_{0H_2} (J/mol)	K_{0CO_2} (1/MPa)	ΔH_{0CO_2} (J/mol)	K_{0H_2O} (1/MPa)	ΔH_{0H_2O} (J/mol)	K_{0CH_3OH} (1/MPa)	ΔH_{0CH_3OH} (J/mol)	K_{0CO} (1/MPa)	ΔH_{0CO} (J/mol)
3.1×10^{-7}	−5726	2.6×10^{-6}	−5410	3.0×10^{-7}	−11,410	4.5×10^{-6}	−10,605	8.1×10^{-7}	−11,150
Confidence interval for:									
$k_{01} = \pm 1 \times 10^5$, $k_{02} = \pm 1 \times 10^6$ K_{0H_2} , K_{0H_2O} , $K_{0CC} = \pm 1 \times 10^{-5}$ K_{0CO_2} , K_{0CH_3OH} , $K_{0CC} = \pm 1 \times 10^{-4}$									
$E_1, E_2, \Delta H_{0H_2}, \Delta H_{0CO_2}, \Delta H_{0H_2O}, \Delta H_{0CH_3OH}, \Delta H_{0CO} = \pm 100$									

The estimated activation energies E_1 and E_2 (Table 4) compared to those determined by Skrzypek et al. [38] (Table 1) are lower, for reaction (1) by about 40% and for reaction (2) by just over 20%. These differences may be due to the difference in the specificity of the catalyst used in the present study (Cu/Zn/Zr/Ga) compared to the Błasiak catalyst (Table 1). The Cu/Zn/Zr/Ga catalyst shows greater resistance to higher concentrations of CO_2 in the synthesis gas and to water formed in the process than the Błasiak catalyst [53]. According to ICI's UK patent [54], methanol synthesis using a low-pressure method on a copper–zinc catalyst modified with, inter alia, chromium can be carried out in the presence of H_2 and CO with no more than 2% CO_2 addition due to the risk of catalyst deactivation. Furthermore, according to studies by Toyira et al. [55,56], the addition of gallium oxide improves the copper dispersion and its stabilisation by achieving a Cu^0/Cu^+ ratio that is optimal for the productivity and lifetime of the catalyst. Ladera et al. [35], while investigating the methanol synthesis from CO_2 and H_2 on a Cu/Zn/Zr/Ga catalyst for other process conditions, obtained for reaction (1) a doubly lower activation energy, and for reaction (2) an activation energy almost one and a half times higher. Moreover, they obtained much higher differences between the activation energies of both reactions, reaching as far as 80,000 J/mol (Table 1). It is worth noting that the kinetic equations obtained by Ladera et al. [35] were in the form of a power monomial with fractional exponents, without taking into account the sorption group. Additionally, the presence of fractional exponents of powers at partial pressures for hydrogen and carbon dioxide in their work indicates a non-elementary course of both

reactions. Analysing the data in Table 4, it can also be seen that the adsorption heats of carbon dioxide and hydrogen are similar and almost half the sorption heat of CO.

The average relative error of the model's fit to experimental results data was 18% for 59 measurement points.

3. Materials and Methods

3.1. Materials

The salts used for the catalyst synthesis were $\text{Cu}(\text{NO}_3)_2 \cdot 3\text{H}_2\text{O}$, $\text{Zn}(\text{NO}_3)_2 \cdot 6\text{H}_2\text{O}$, $\text{ZrO}(\text{NO}_3)_2 \cdot \text{H}_2\text{O}$, and $\text{Ga}(\text{NO}_3)_3 \cdot x\text{H}_2\text{O}$ from Sigma-Aldrich USA (St. Louis, MO, USA); the citric acid monohydrate was from StanlabSp.j. Poland; 65% nitric acid (V) was from Avantor Performance Materials Poland; all reagents were of analytical purity.

The carbon dioxide, hydrogen, carbon monoxide, and nitrogen that were used in the preparation of gas mixtures for kinetic studies were from SIAD; all the gases were of technical purity.

3.2. Catalyst Preparation

The Cu/Zn/Zr/Ga catalyst was prepared by a citric acid homogenisation method called the "citrate method" [57]. The reason we used this method was to obtain perfectly mixed components thanks to the branched structure of citrates and consequently excellent homogeneity and fully repeatable properties of the prepared catalyst [58]. The conventional method of co-precipitation did not provide such results, although it is usually used, as it is described in the literature.

Stoichiometric amounts of Cu, Zn, Zr, and Ga nitrates were carefully added to a citric acid solution ($2 \text{ mol/dm}^3 + 2\%$ excess). The composition of the obtained Cu/Zn/Zr/Ga catalyst was 65.3/26.3/4.5/3.9 (wt.%). The mixture was then evaporated in a rotary vacuum evaporator at 380 K for about 24 h. The resulting metal citrate precipitate was carefully oxidised to ensure that local overheating and explosive oxidation reactions were prevented (temperature programme: 360 K, 0.1 K/min; 403 K). The resulting oxide mixture was roasted in a muffle furnace with air access (temperature program: 373 K, 473 K, 523 K, 573 K, and 623 K for 1 h). The final stages of preparation were tableting of the obtained powder and crushing and sieving to obtain the desired grain size (0.8–1 mm grain) [58].

3.3. Catalysts Characterization

Phase analysis based on X-ray powder diffraction (XRD) measurements was performed on a Bruker D8 Advance diffractometer with a Lynx Eye detector and Johansson monochromator, working in Bragg–Brentano geometry. The XRD measurements (at 40 kV and 30 mA) were performed in the 2θ range from 5° to 90° with the interpolated step size 0.02° . The crystallite sizes were calculated using the Scherrer method. XRD phase analysis was performed using reference standards from the International Centre for Diffraction Data (ICDD) PDF-4 database.

The BET surface area was measured with nitrogen adsorption at 77 K using Quantachrome Autosorb-1. Prior to the measurements, samples were preheated and degassed under vacuum at 373 K for 18 h. The pore size distribution profiles were obtained by using the Barrett–Joyner–Halenda (BJH) method from the desorption branch. The micropore area was obtained by using the V–t plot method.

The active surface of copper (S_{Cu}) in the reduced catalyst was determined with the use of reactive adsorption of N_2O at 363 K (VG/Fisons Quartz 200D) according to the method described in [59]. It has been assumed in calculations that the reoxidation of surface copper follows the chemical equation $2\text{Cu}(\text{s}) + \text{N}_2\text{O}(\text{g}) \rightarrow \text{Cu}_2\text{O}(\text{s}) + \text{N}_2(\text{g})$ and that 1 m^2 of elemental copper corresponds to $6.1 \mu\text{mol}$ of O_2 .

The CO_2 TPD (CO_2 temperature-programmed desorption) measurements were carried out in a quartz fixed-bed flow reactor connected online to a mass spectrometer (QMG 220 PRISMA PLUS). Prior to the TPD run, the sample (50 mg) was reduced in 5% H_2/Ar flow at 723 K for 1 h. Next, the reactor was cooled down to room temperature (RT) and pulses

(250 μL) of 5% CO_2/Ar were introduced until saturation. Then, the sample was flushed with He flow (40 mL/min) for 0.5 h until a stable CO_2 line ($m/z = 44$) was obtained. TPD was performed from RT to 973 K with $\Delta T = 10$ K/min under He flow.

TG measurements were carried out on a STAR 850 Mettler Toledo apparatus in nitrogen and air, in the temperature range of 298–773 K with a linear temperature rise (10 K/min) and gas flow rate of 60 cm^3/min .

3.4. Kinetic Tests

Kinetic tests were performed in the continuous-flow fixed-bed stainless steel reactor of 18 cm length and 1.3 cm inner diameter. The 2 g of the catalyst was placed between two layers of ceramic grains. After leaving the reactor, the reaction mixture was analysed with the Varian Star 3800 gas chromatograph. The methanol content was determined by the flame ionisation detector (FID) with CP-Wax column. Gases were analysed by the thermalconductivity detector (TCD) with the Carbo Plot column; additionally, carbon compounds were determined quantitatively in the methanizer. To activate the catalyst, reduction of the oxidised form of the catalyst was performed in a stream of dilute hydrogen (gas flow 50 mL/min, 7% H_2 in N_2) at 473 K under atmospheric pressure for 2 h. Schematic of the apparatus is shown in Figure 13.

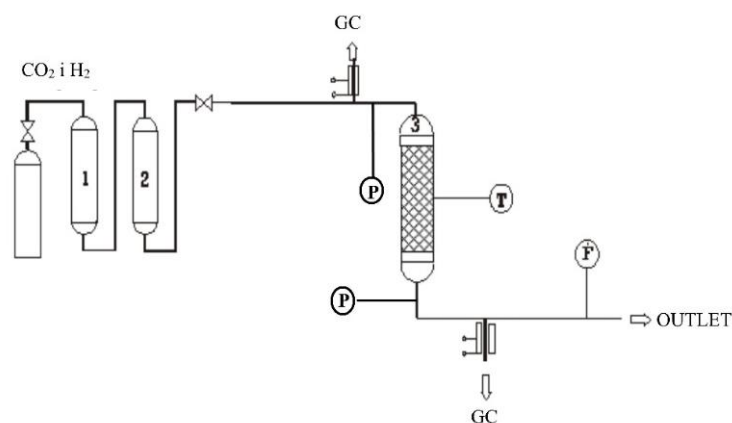


Figure 13. Scheme of experimental system: 1—deoxidizer (BTS), 2—dryer, 3—reactor, GC—gas chromatograph, T—thermocouple, F—flowmeter, P—manometers.

Before starting the kinetic studies, it was necessary to stabilise the catalyst. This stabilisation was carried out in a reaction mixture consisting of 70 mol% H_2 and 20 mol% CO_2 and nitrogen, for a GHSV of 3300 1/h at 4 MPa, according to a temperature program: 443 K, 1.5 deg/min; 553 K for 4 h. Kinetic studies were carried out under the conditions shown in Table 5.

Table 5. Conditions for performing kinetic studies.

Parameter	Value
T (K)	433–513
p_c (MPa)	3–8
GHSV (1/h)	1660–10,000
Inlet gas composition (-)	
H_2	0.30–0.71
CO_2	0.05–0.23
CO	0.00–0.06
N_2	0.05–0.49

On the basis of the experimental data obtained, the following were calculated:

(a) conversion degrees (α_1^{exp} , α_2^{exp}) from the formulae:
for reaction (1)

$$\alpha_1^{\text{exp}} = \frac{\dot{F}_{\text{MeOH}}}{\dot{F}_{\text{CO}} + \dot{F}_{\text{CO}_2}}, \quad (10)$$

for reaction (2)

$$\alpha_2^{\text{exp}} = \frac{\dot{F}_{\text{CO}} - \dot{F}_{\text{CO}}^0}{\dot{F}_{\text{CO}} + \dot{F}_{\text{CO}_2}}, \quad (11)$$

(b) productivity (P_{MeOH}):

$$P_{\text{MeOH}} = \frac{\dot{F}_{\text{MeOH}} \cdot M_{\text{MeOH}}}{m_{\text{cat}}}. \quad (12)$$

The integrative method was used to check the potential kinetic model. The kinetic data obtained were compared with the data obtained from the solution of differential equations, which are in fact the mass balance for the tubular reactor:

$$\frac{d\alpha_1}{d\tau} = \frac{r_1 \cdot m_{\text{cat}}}{(x_{\text{CO}_2}^0 + x_{\text{CO}}^0) \cdot F_{0n}}, \quad (13)$$

$$\frac{d\alpha_2}{d\tau} = \frac{r_2 \cdot m_{\text{cat}}}{(x_{\text{CO}_2}^0 + x_{\text{CO}}^0) \cdot F_{0n}}. \quad (14)$$

The analysed forms of kinetic equations were inserted in place of r_1 and r_2 in Equations (13) and (14). The obtained differential Equations (13) and (14) were integrated using the numerical method of Runge and Kutta IV, and the calculated values of the α_1^{cal} and α_2^{cal} were compared with the corresponding experimental values α_1^{exp} and α_2^{exp} .

The model for experimental data fitting was evaluated by the mean relative error determined by the following formula:

$$k_{\text{on}}, E_n, K_{0i}, \Delta H_{0i} = \arg \min \sum_{j=1}^A \sum_{l=1}^B \text{abs} \frac{\alpha_{jl}^{\text{cal}} - \alpha_{jl}^{\text{exp}}}{\alpha_{jl}^{\text{exp}}}. \quad (15)$$

The Levenberg–Marquardt nonlinear regression method was used to simultaneously determine the above parameter values. The algorithm was modified to adjust it to any objective function. The program code was written in BASIC.

4. Summary

This paper presents kinetic investigations on the methanol synthesis from carbon dioxide and hydrogen in a continuous-flow fixed-bed reactor in the presence of a Cu/Zn/Zr/Ga catalyst. The study showed strong effects of temperature and initial molar fractions of hydrogen and carbon dioxide and weak effects of pressure, GHSV, and initial molar fraction of CO on the conversion degrees α_1^{exp} and α_2^{exp} . The Cu/Zn/Zr/Ga catalyst showed good stability over 960 h.

The kinetics of the investigated process can be described by determined in this work kinetic equations of the Langmuir–Hinshelwood type, with the surface reaction between carbon dioxide and hydrogen as the limiting step. The average relative error of fitting the kinetic equations to the experimental data was 18%.

Due to the wide range of process parameters studied, the proposed kinetic equations can be used in design and optimization of industrial-scale chemical reactors manufacturing methanol.

Author Contributions: Conceptualization, M.M.-L., Ł.H. and M.G.; methodology, M.G.; software, M.G.; investigation, Ł.H. and M.Ś.; data curation, Ł.H., M.Ś. and M.M.-L.; writing—Ł.H., M.M.-L., M.G. and M.Ś.; original draft preparation, Ł.H., M.M.-L. and M.G.; writing—review and editing, Ł.H., M.M.-L., M.G. and M.Ś.; supervision, M.M.-L. and M.G. All authors have read and agreed to the published version of the manuscript.

Funding: This research received no external funding.

Data Availability Statement: Institute of Chemical Engineering, Polish Academy of Sciences, 5 Bałtycka Street, 44-100 Gliwice, Poland and Jerzy Haber Institute of Catalysis and Surface Chemistry, Polish Academy of Sciences, 8 Niezapominajek Street, 30-239 Krakow, Poland.

Conflicts of Interest: The authors declare no conflict of interest.

Nomenclature

A	total number of chemical reactions, $A = 2$ (Equation (15))
B	total number of measurement points, $B = 59$ (Equation (15))
E	activation energy of reaction n, J/mol
\dot{F}_i	molar flow rate of reactant i, mol/h
GHSV	gas hourly space velocity, 1/h
k_0	pre-exponential factor of reaction n
K_0	initial adsorption constant of reactant i, 1/MPa
M	molar mass, g/mol
m	mass of catalyst, g
p	pressure, Pa
R	ideal gas constant, 8.314 J/mol·K
T	temperature, K
Tot	Total
x	mole fraction of reactanti
Greek symbols	
Δh	reaction enthalpy, J/mol
ΔH	adsorption enthalpy of reactanti, J/mol
τ	spacetime
superscripts	
0	initial state
a, b	exponents in the kinetic equations (sorption group)
cal	calculated value
exp	experimental value
subscripts	
1	first reaction
2	second reaction
ads	adsorption
c	total mass or pressure
cat.	catalyst
des	desorption
i	reactanti = CO ₂ , H ₂ , CO, CH ₃ OH, H ₂ O
j	number of reaction (1 or 2) in Equation (15)
l	number of measuring points in Equation (15)
MeOH	methanol
n	reaction n (1 or 2)

References

1. Murthy, P.S.; Liang, W.; Jiang, Y.; Huang, J. Cu-Based Nanocatalysts for CO₂ Hydrogenation to Methanol. *Energy Fuels* **2021**, *35*, 8558–8584. [CrossRef]
2. Samimi, F.; Rahimpour, M.R.; Shariati, A. Development of an Efficient Methanol Production Process for Direct CO₂ Hydrogenation over a Cu/ZnO/Al₂O₃ Catalyst. *Catalysts* **2017**, *7*, 332. [CrossRef]
3. Wei, X.; Cao, S.; Wei, S.; Liu, S.; Wang, Z.; Dai, F.; Lu, X. Theoretical investigation on electrocatalytic reduction of CO₂ to methanol and methane by bimetallic atoms TM1/TM2-N@Gra (TM = Fe, Co, Ni, Cu). *Appl. Surf. Sci.* **2022**, *593*, 153377–153386. [CrossRef]
4. Siakavelas, G.I.; Charisiou, N.D.; Alkhoori, A.; Alkhoori, S.; Sebastian, V.; Hinder, S.J.; Baker, M.A.; Yentekakis, I.V.; Polychronopoulou, K.; Goula, M.A. Highly selective and stable Ni/La-M (M = Sm, Pr, and Mg)-CeO₂ catalysts for CO₂ methanation. *J. CO₂ Util.* **2021**, *51*, 101618–101638. [CrossRef]
5. Liu, K.; Xu, X.; Xu, J.; Fang, X.; Liu, L.; Wang, X. The distributions of alkaline earth metal oxides and their promotional effects on Ni/CeO₂ for CO₂ methanation. *J. CO₂ Util.* **2020**, *38*, 113–124. [CrossRef]
6. Shinde, G.Y.; Mote, A.S.; Gawande, M.B. Recent Advances of Photocatalytic Hydrogenation of CO₂ to Methanol. *Catalysts* **2022**, *12*, 94. [CrossRef]
7. Xu, D.; Hong, X.; Liu, G. Highly dispersed metal doping to ZnZr oxide catalyst for CO₂ hydrogenation to methanol: Insight into hydrogen spillover. *J. Catal.* **2021**, *393*, 207–214. [CrossRef]
8. Stawowy, M.; Ciesielski, R.; Maniecki, T.; Matus, K.; Łuźny, R.; Trawczynski, J.; Silvestre-Albero, J.; Łamacz, A. CO₂ Hydrogenation to Methanol over Ce and Zr Containing UiO-66 and Cu/UiO-66. *Catalysts* **2020**, *10*, 39. [CrossRef]
9. Dalena, F.; Senatore, A.; Marino, A.; Gordano, A.; Basile, M.; Basile, A. *The Science and Engineering of Methanol*; Basile, A., Dalena, F., Eds.; Elsevier: Amsterdam, The Netherlands, 2017; Chapter 1; pp. 3–28.
10. Gómez, D.; Candia, C.; Jiménez, R.; Karelovic, A. Isotopic transient kinetic analysis of CO₂ hydrogenation to methanol on Cu/SiO₂ promoted by Ga and Zn. *J. Catal.* **2022**, *406*, 96–106. [CrossRef]
11. Stangeland, K.; Navarro, H.H.; Huynh, H.L.; Tucho, W.M.; Yu, Z. Tuning the interfacial sites between copper and metal oxides (Zn, Zr, In) for CO₂ hydrogenation to methanol. *Chem. Eng. Sci.* **2021**, *238*, 116603. [CrossRef]
12. Fujitani, T. Enhancement of the Catalytic Performance and Active Site Clarification of Cu/ZnO Based Catalysts for Methanol Synthesis by CO₂ Hydrogenation. *J. Jpn. Pet. Inst.* **2020**, *63*, 43–51. [CrossRef]
13. Witoon, T.; Numpilai, T.; Phongamwong, T.; Donphai, W.; Boonyuen, C.; Warakulwit, C.; Chareonpanich, M.; Limtrakul, J. Enhanced activity, selectivity and stability of a CuO-ZnO-ZrO₂ catalyst by adding graphene oxide for CO₂ hydrogenation to methanol. *Chem. Eng. J.* **2018**, *334*, 1781–1791. [CrossRef]
14. Chang, K.; Wang, T.; Chen, J.G. Hydrogenation of CO₂ to methanol over CuCeTi-Ox catalysts. *Appl. Catal. B Environ.* **2017**, *206*, 704–711. [CrossRef]
15. Alias, M.S.; Kamarudin, S.K.; Zainoodin, A.M.; Masdar, M.S. Active direct methanol fuel cell: An overview. *Int. J. Hydrogen Energy* **2020**, *45*, 19620–19641. [CrossRef]
16. Natesakhawat, S.; Lekse, J.W.; Baltrus, J.P.; Ohodnicki, P.R., Jr.; Howard, B.H.; Deng, X.; Matranga, C. Active Sites and Structure–Activity Relationships of Copper-Based Catalysts for Carbon Dioxide Hydrogenation to Methanol. *ACS Catal.* **2012**, *2*, 1667–1676. [CrossRef]
17. Dana, M.S.; Emeric, S.; Ómar, S. Process Advantages of Direct CO₂ to Methanol Synthesis. *Front. Chem.* **2018**, *6*, 446–453. [CrossRef]
18. Ushikoshi, K.; Moria, K.; Watanabe, T.; Takeuchi, M.; Saito, M. A 50 kg/day class test plant for methanol synthesis from CO₂ and H₂. *Stud. Surf. Sci. Catal.* **1998**, *114*, 357–362. [CrossRef]
19. Production of Renewable Methanol from Captured Emissions and Renewable Energy Sources, for Its Utilisation for Clean Fuel Production and Green Consumer Goods. Available online: <https://cordis.europa.eu/project/id/848757> (accessed on 21 January 2022).
20. Methanol Production Capacity May Quintuple on Decarbonized Industry Transformation: Study. Available online: <https://cleanenergynews.ihsmarkit.com/research-analysis/methanol-production-capacity-may-quintuple-on-decarbonized-ind.html> (accessed on 21 January 2022).
21. Goehna, H.; Koenig, P. Producing methanol from CO₂. *Chemtech* **1994**, *24*, 36–38.
22. Herman, R.G.; Klier, K.; Simmons, G.W.; Finn, B.P.; Bulko, J.B.; Kobylinski, T.P. Catalytic synthesis of methanol from CO₂: I. Phase composition, electronic properties, and activities of the Cu/ZnO/M₂O₃ catalysts. *J. Catal.* **1979**, *56*, 407–429. [CrossRef]
23. Brown, N.J.; Weiner, J.; Hellgardt, K.; Shaffer, M.S.P.; Williams, C.K. Phosphinate stabilized ZnO and Cu colloidal nanocatalysts for CO₂ hydrogenation to methanol. *Chem. Commun.* **2013**, *49*, 11074–11076. [CrossRef]
24. Richard, A.R.; Fan, M. Rare earth elements: Properties and applications to methanol synthesis catalysis via hydrogenation of carbon oxides. *J. Rare Earth.* **2018**, *36*, 1127–1135. [CrossRef]
25. Spadaro, L.; Palella, A.; Arena, F. Totally-green Fuels via CO₂ Hydrogenation. *Bull. Chem. React. Eng. Catal.* **2020**, *15*, 390–404. [CrossRef]
26. Arena, F.; Barbera, K.; Italiano, G.; Bonura, G.; Spadaro, L.; Frusteri, F. Synthesis, characterization and activity pattern of Cu–ZnO/ZrO₂ catalysts in the hydrogenation of carbon dioxide to methanol. *J. Catal.* **2007**, *249*, 185–194. [CrossRef]
27. Din, U.; Shaharun, M.S.; Subbarao, D.; Naeem, A.; Hussain, F. Influence of niobium on carbon nanofibres based Cu/ZrO₂ catalysts for liquid phase hydrogenation of CO₂ to methanol. *Catal. Today* **2016**, *259*, 303–311. [CrossRef]

28. Huang, X.; Ma, L.; Wainwright, M.S. The influence of Cr, Zn and Co additives on the performance of skeletal copper catalysts for methanol synthesis and related reactions. *Appl. Catal. A Gen.* **2004**, *257*, 235–243. [[CrossRef](#)]
29. Fujitani, T.; Saito, M.; Kanai, Y.; Takeuchi, M.; Moria, K.; Watanabe, T.; Kawai, M.; Kakumoto, T. Methanol Synthesis from CO₂ and H₂ over Cu/ZnO/Ga₂O₃ Catalyst. *Chem. Lett.* **1993**, *22*, 1079–1080. [[CrossRef](#)]
30. Li, C.M.; Yuan, X.D.; Fujimoto, K. Development of highly stable catalyst for methanol synthesis from carbon dioxide. *Appl. Catal. A Gen.* **2014**, *469*, 306–311. [[CrossRef](#)]
31. Słoczyński, J.; Grabowski, R.; Olszewski, P.; Kozłowska, A.; Stoch, J.; Lachowska, M.; Skrzypek, J. Effect of metal oxide additives on the activity and stability of Cu/ZnO/ZrO₂ catalysts in the synthesis of methanol from CO₂ and H₂. *Appl. Catal. A Gen.* **2006**, *310*, 127–137. [[CrossRef](#)]
32. Ban, H.Y.; Li, C.M.; Asami, K.; Fujimoto, K. Influence of rare-earth elements (La, Ce, Nd and Pr) on the performance of Cu/Zn/Zr catalyst for CH₃OH synthesis from CO₂. *Catal. Commun.* **2014**, *54*, 50–54. [[CrossRef](#)]
33. Hamryszak, Ł.; Madej-Lachowska, M.; Grzesika, M.; Kocot, K.; Ruggiero-Mikołajczyk, M. Wpływ dodatku Ce, Cr i/lub Ga do katalizatora Cu/Zn/Zr na synteze metanolu z ditlenku węgla i wodoru. *Przem. Chem.* **2019**, *98*, 133–137. [[CrossRef](#)]
34. Madej-Lachowska, M.; Kasprzyk-Mrzyk, A.; Lachowski, A.; Wyżgoł, H. Synteza metanolu z ditlenku węgla i wodoru na bazie katalizatora CuO/ZnO/ZrO₂ z dodatkami. *Chemik* **2014**, *68*, 61–64.
35. Ladera, R.; Pérez-Alonso, F.J.; González-Carballo, J.M.; Ojeda, M.; Rojas, S.; Fierro, J.L.G. Catalytic valorization of CO₂ via methanol synthesis with Ga-promoted Cu–ZnO–ZrO₂ catalysts. *Appl. Catal. B Environ.* **2013**, *142–143*, 241–248. [[CrossRef](#)]
36. Graaf, G.H.; Stamhuis, E.J.; Beenackers, A.A.C.M. Kinetics of low-pressure methanol synthesis. *Chem. Eng. Sci.* **1988**, *43*, 3185–3195. [[CrossRef](#)]
37. Malinovskaya, O.A.; Rozovskii, A.Y.; Zolotarskii, I.A.; Lender, Y.V.; Matros, Y.S.; Lin, G.I.; Dubovich, G.V.; Popova, N.A.; Savostina, N.V. Synthesis of methanol on Cu-based catalyst: Kinetic model. *React. Kinet. Catal. Lett.* **1987**, *34*, 87. [[CrossRef](#)]
38. Skrzypek, J.; Lachowska, M.; Moroz, H. Kinetics of methanol synthesis over commercial copper/zinc oxide/alumina catalysts. *Chem. Eng. Sci.* **1991**, *46*, 2809–2813. [[CrossRef](#)]
39. VandenBussche, K.M.; Froment, G.F. A Steady-State Kinetic Model for Methanol Synthesis and the Water Gas Shift Reaction on a Commercial Cu/ZnO/Al₂O₃ Catalyst. *J. Catal.* **1996**, *161*, 1–10. [[CrossRef](#)]
40. Kubota, T.; Hayakawa, I.; Mabuse, H.; Mori, K.; Ushikoshi, K.; Watanabe, T. Kinetic study of methanol synthesis from carbon dioxide and hydrogen. *Appl. Organomet. Chem.* **2001**, *15*, 121–126. [[CrossRef](#)]
41. Portha, J.-F.; Parkhomenko, K.; Kobl, K.; Roger, A.-C.; Arab, S.; Commenge, J.-M.; Falk, L. Kinetics of Methanol Synthesis from Carbon Dioxide Hydrogenation over Copper–Zinc Oxide Catalysts. *Ind. Eng. Chem. Res.* **2017**, *56*, 13133–13145. [[CrossRef](#)]
42. Marcos, F.C.F.; Cavalcanti, F.M.; Petrolini, D.D.; Lin, L.; Betancourt, L.E.; Senanayake, S.D.; Rodriguez, J.A.; Assaf, J.M.; Giudici, R.; Assaf, E.M. Effect of operating parameters on H₂/CO₂ conversion to methanol over Cu–Zn oxide supported on ZrO₂ polymorph catalysts: Characterization and kinetics. *Chem. Eng. J.* **2022**, *427*, 130947–130961. [[CrossRef](#)]
43. Natesakhawat, S.; Ohodnicki, P.R., Jr.; Howard, B.H.; Lekse, J.W.; Baltrus, J.P.; Matranga, C. Adsorption and deactivation characteristics of Cu/ZnO-based catalysts for methanol synthesis from carbon dioxide. *Top. Catal.* **2013**, *56*, 1752–1763. [[CrossRef](#)]
44. Zhong, C.; Guo, X.; Mao, D.; Wang, S.; Wu, G.; Lu, G. Effects of alkaline-earth oxides on the performance of a CuO–ZrO₂ catalyst for methanol synthesis via CO₂ hydrogenation. *RSC Adv.* **2015**, *5*, 52958–52965. [[CrossRef](#)]
45. Smyrniotis, M.; Tampaxis, C.; Steriotis, T.; Ioannides, T. Study of CO₂ adsorption on a commercial CuO/ZnO/Al₂O₃ catalyst. *Catal. Today* **2020**, *357*, 495–502. [[CrossRef](#)]
46. Śliwa, M.; Socha, R. Modification of CuO–ZrO₂–ZnO Mixed Oxide Catalyst with Mn, Ga, Ni: Impact on Physicochemical Properties and Hydrogen Production via Low Temperature Steam Reforming of Ethanol. *Catal. Lett.* **2022**. [[CrossRef](#)]
47. Zhang, S.; Fortier, H.; Dahn, J.R. Characterization of zinc carbonate hydroxides synthesized by precipitation from zinc acetate and potassium carbonate solutions. *Mater. Res. Bull.* **2004**, *39*, 1939–1948. [[CrossRef](#)]
48. Zhao, Y.; Li, Y.; He, Z.; Yan, Z. Facile preparation of Cu/Cu₂O nanoporous nanoparticles as a potential catalyst for non-enzymatic glucose sensing. *RSC Adv.* **2013**, *3*, 2178–2181. [[CrossRef](#)]
49. Wang, G.; Mao, D.; Guo, X.; Yu, J. Enhanced performance of the CuO–ZnO–ZrO₂ catalyst for CO₂ hydrogenation to methanol. By WO₃ modification. *Appl. Surf. Sci.* **2018**, *456*, 403–409. [[CrossRef](#)]
50. Gaikwad, R.V. Carbon Dioxide to Methanol: Stoichiometric Catalytic Hydrogenation under High Pressure Conditions. Ph.D. Thesis, University Rovira and Virgili, Tarragona, Spain, 2018.
51. Ash-Kurlander, U.; Martin, O.; Fontana, L.D.; Patil, V.R.; Bernegger, M.; Mondelli, C.; Pérez-Ramírez, J.; Steinfeld, A. Impact of Daily Startup–Shutdown Conditions on the Production of Solar Methanol over a Commercial Cu–ZnO–Al₂O₃ Catalyst. *Energy Technol.* **2016**, *4*, 565–572. [[CrossRef](#)]
52. Janiczek, W. Synteza metanolu na tle układu C–H–O. *Czas. Tech. Chem.* **2010**, *10*, 108–122.
53. Lachowska, M.; Skrzypek, J. Ga, Mn and Mg promoted copper/zinc/zirconia—Catalysts for hydrogenation of carbon dioxide to methanol. *Studies Surf. Sci. Catal.* **2004**, *153*, 173–176.
54. Davies, P.; Snowdon, F.F.; Bridger, G.W.; Hughes, D.P.; Young, P.W. Water-Gas Conversion and Catalysts Therefor. UK Patent 1010871, 24 November 1965.
55. Toyir, J.; de la Piscina, P.R.; Fierro, J.L.G.; Homs, N. Highly effective conversion of CO₂ to methanol over supported and promoted copper-based catalysts: Influence of support and promoter. *Appl. Catal. B Environ.* **2001**, *29*, 207–215. [[CrossRef](#)]

56. Toyir, J.; de la Piscina, P.R.; Fierro, J.L.G.; Homs, N. Catalytic performance for CO₂ conversion to methanol of gallium-promoted copper-based catalysts: Influence of metallic precursors. *Appl. Catal. B Environ.* **2001**, *34*, 255–266. [[CrossRef](#)]
57. Courty, P.; Ajoy, H.; Marcilly, C.; Delmon, B. Oxydes mixtes ou en solution solide sous forme très divisée obtenus par décomposition thermique de précurseurs amorphes. *Powder Technol.* **1973**, *7*, 21–38. [[CrossRef](#)]
58. Lachowska, M. Steam reforming of methanol over Cu/Zn/Zr/Ga catalyst: Effect of the reduction conditions on the catalytic performance. *Reac. Kinet. Mech. Cat.* **2010**, *101*, 85–91. [[CrossRef](#)]
59. Hamryszak, Ł.; Kulawska, M.; Madej-Lachowska, M.; Ruggiero-Mikołajczyk, M.; Samson, K.; Śliwa, M. Copper Tricomponent Catalysts Application for Hydrogen Production from Ethanol. *Catalysts* **2021**, *11*, 575. [[CrossRef](#)]